Supporting information

Unidirectional Doubly Enhanced MoS_2 Emission via Photonic Fano Resonances

Xingwang Zhang[†], *Shinhyuk Choi*[‡], *Dake Wang*[†], *Carl H. Naylor*[||], *A. T. Charlie Johnson*[||], *and Ertugrul Cubukcu*[†,‡,*]

[†]Department of Nanoengineering, [‡]Department of Electrical and Computer Engineering, University of California, San Diego, La Jolla, California 92093, United States

[||]Department of Physics and Astronomy, University of Pennsylvania, Philadelphia, Pennsylvania 19104, United States

KEYWORDS: Fano resonance, photonic crystal, Molybdenum disulfide, 2D materials, photoluminescence, unidirectional emission

Corresponding Author *E-mail: ecubukcu@ucsd.edu.

Contents

1. The design of photonic crystal (PhC) slab

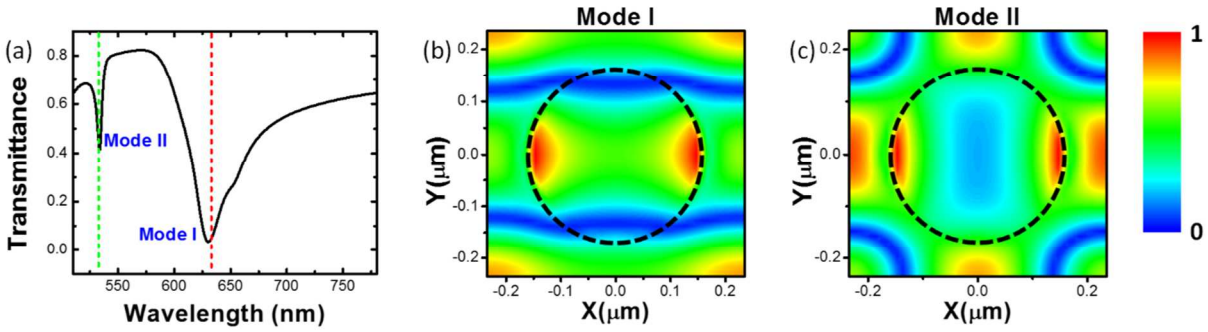

Figure S1. Fano resonances of the SiN photonic crystal (PhC) slab integrated with the MoS_2 monolayer. (a) Simulated transmittance spectrum of the device (PhC period: Λ=470 nm, SiN thickness: h=100 nm, hole radius: r=160 nm). Two resonance dips are identified as Mode I and Mode II respectively, which overlap with the wavelengths of the 532 nm (green dashed line) and 633 nm (red dashed line) pump lasers used in the experiment; the FDTD calculated electric field profile ($|E_x|$) in the center plane (XY plane) of the SiN slab for Mode I (b) and Mode II (c). The dashed circles indicate the outline of the holes.

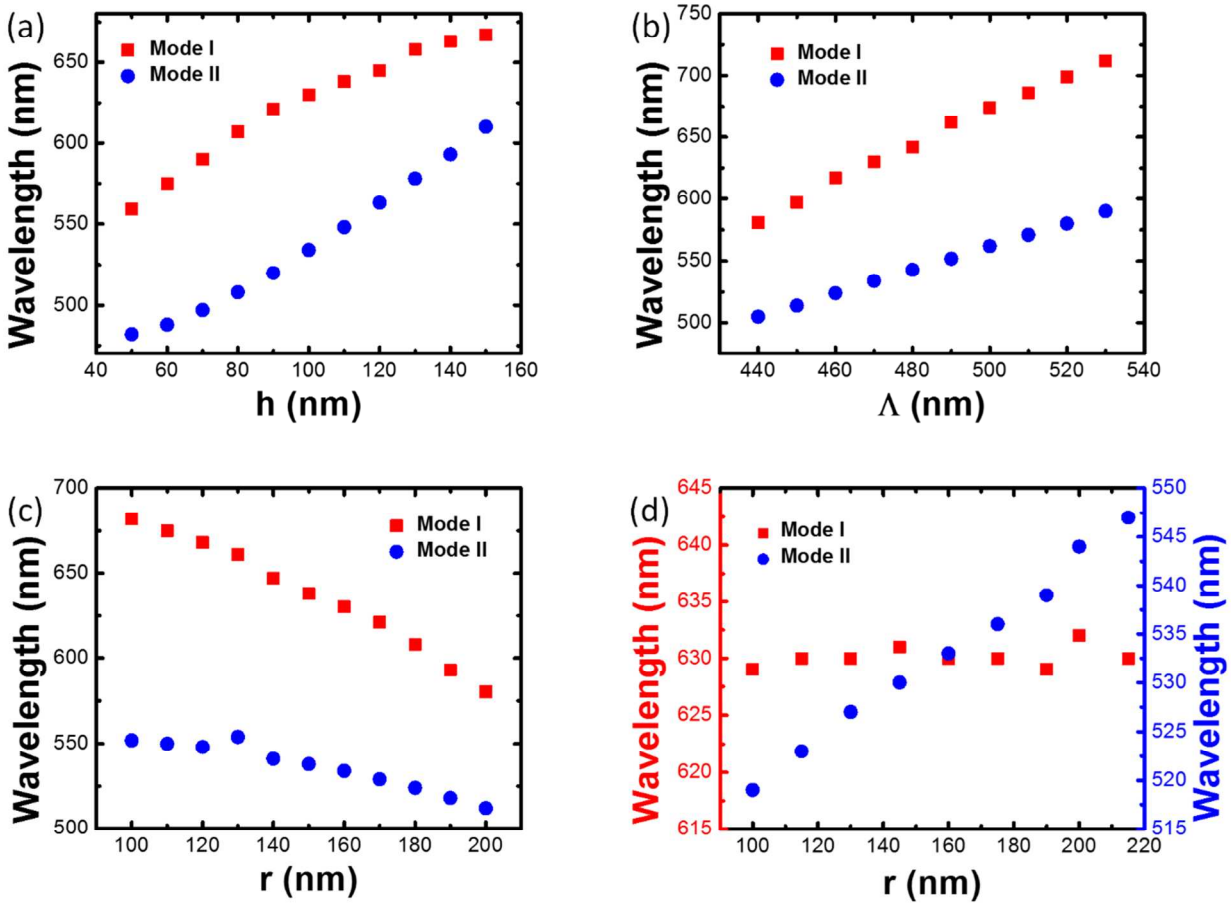

Figure S2. The design of the SiN PhC slab integrated with the MoS_2 monolayer. (a) The FDTD calculated wavelengths of Mode I and Mode II as a function of (a) SiN thickness for constant PhC period Λ=470 nm and the hole radius r=160 nm; (b) hole period for constant SiN thickness h=100 nm and r=160 nm; (c) hole radius for constant h=100 nm and Λ=470 nm. (d) A resonance near 630 nm can be achieved with various parameter configurations for constant h=100 nm. The data represent nine sets of parameters: Λ=430 nm, r=100 nm; Λ=440 nm, r=115 nm; Λ=450 nm, r=130 nm; Λ=460 nm, r=145 nm; Λ=470 nm, r=160 nm; Λ=480 nm, r=175 nm; Λ=490 nm, r=190 nm; Λ=500 nm, r=200 nm; Λ=510 nm, r=215 nm.

As can be seen in Fig. S1, the MoS_2-PhC hybrid resonator (PhC period: Λ=470 nm, SiN thickness: h=100 nm, hole radius: r=160 nm) has Fano resonances at both 532 nm and 633 nm, which are consistent with the wavelengths of the pump lasers we used in the experiment. Therefore, the device has resonant absorption enhancement for both 532 nm and 633 nm pump lasers. To achieve this, we have optimized the PhC slab parameters by following the procedure as described below:

1. As shown in Fig S2, both Mode I and Mode II of the PhC slab have red shifts when the SiN thickness and hole period increase, while having blueshifts when the hole radius increases. For the commercially available SiN membrane we used, the thickness (h) is 100 nm. To achieve the highest MoS_2 photoluminescence enhancement, we have optimized both the radius of the hole (r) and PhC period (Λ).

2. We tuned the PhC period for different radii of the holes to make sure the MoS_2-PhC hybrid resonators have Fano resonances at both 532 nm and 633 nm. As shown in Fig. S2d, when the radius of the hole r=160 nm and period Λ=470 nm, the MoS_2-PhC hybrid resonator has Fano resonances for both the pump lasers.

3. Due to the lack of n-doping and defect-assisted non-radiative exciton recombination from the substrate, the suspended part of the MoS_2 monolayer has a higher quantum yield compared to that on the SiN substrate. Therefore, to obtain a higher intrinsic quantum yield (i.e. chemical enhancement), we need a higher filling fraction $\pi r^2/\Lambda^2$. However, if the filling fraction is too high, the SiN frame becomes too narrow to withstand the MoS_2 monolayer transfer process. For the radius and period we chose in the experiment (Λ=470 nm, r=160 nm), the filling

fraction is 0.36, which is relatively high for a structurally robust SiN PhC frame to achieve a high chemical enhancement.

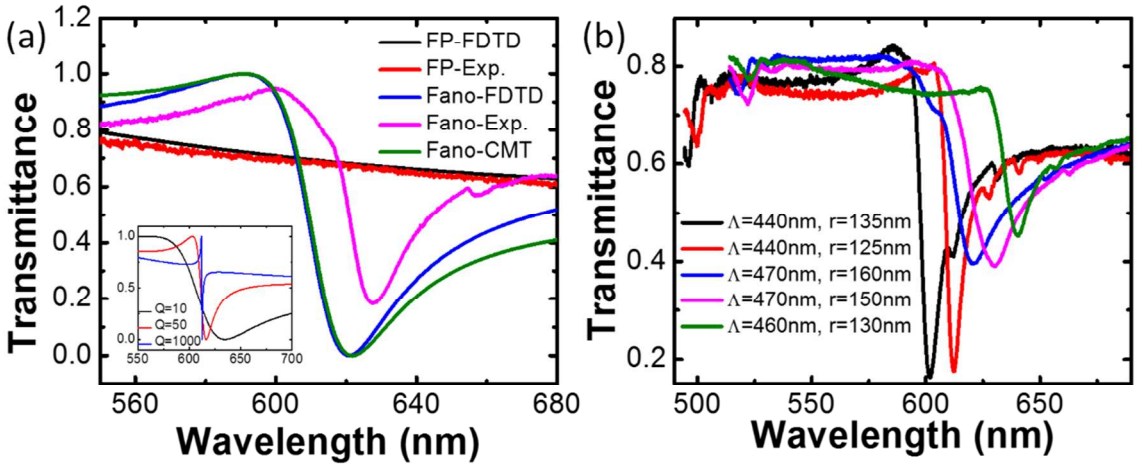

Figure S3. (a) The Fano resonances in the PhC slab. FP-FDTD: calculated Fabry–Pérot interference background for the unpatterned SiN slab by the FDTD; FP-Exp.: measured Fabry–Pérot interference spectrum; Fano-FDTD: calculated PhC Fano resonance by the FDTD; Fano-CMT: calculated PhC Fano resonance by the temporal coupled-mode theory. Inset: Comparison of the Fano resonance lineshapes for PhC guided resonances of different quality factors (Q). It can be seen that a Q around 50 yields a lineshape very similar to the experimental result (Fano-Exp). (b) Measured PhC Fano resonances for various samples. The Fano resonance can be widely tuned by adjusting the PhC period (Λ) and the radius (r) of the hole.

As discussed in the main text, the Fano resonances in the PhC slab arises from the coupling between the PhC guided resonances and the Fabry–Pérot interference of the SiN slab, which can be described by the temporal coupled-mode theory[1]:

$$\frac{da}{dt} = \left(j\omega_0 - \frac{1}{\tau}\right) \cdot a + \kappa \cdot s_+, \tag{S-1}$$

$$s_- = C_s \cdot s_+ + C_a \cdot a, \tag{S-2}$$

where, Eq. (S-1) describes the time dependent amplitude of a PhC guided resonance (a) with the resonance frequency ω_0 and the life time τ. The amplitude of the PhC guided resonance is modified due to the coupling of the Fabry–Pérot interference of the SiN slab, and κ is the coupling coefficient. On the other hand, the PhC guided resonance can also modify the Fabry–Pérot interference, which is expressed by Eq. (S-2). s_+, s_-, C_s and C_a are the incident and reflected light amplitudes, the coupling coefficients from the incident light and the PhC resonance, respectively. Therefore, we can derive the transmittance of the PhC[1],

$$T = 1 - \frac{r^2(\omega-\omega_0)^2+t^2(1/\tau)^2-2rt(\omega-\omega_0)(1/\tau)}{(\omega-\omega_0)^2-(1/\tau)^2}. \tag{S-3}$$

where, *r* and *t* are respectively the reflection and transmission amplitude coefficients of the SiN slab.

As shown in Fig. S3a, measured Fabry–Pérot (FP) transmission spectrum of the unpatterned SiN slab agrees well with the FDTD calculated results. In the meantime, we extract the PhC guided resonance frequency ω_0 and the life time τ from the electric field temporal decay after the pulse excitation in the FDTD simulation. Then we can calculate the transmittance of the PhC slab by using Eq. (S-3), and an asymmetric line shape (i.e. Fano resonance) appears due to the coupling of the PhC guided resonance and the FP interference, which agrees with the FDTD simulation results very well (Fig. S3a). In the experiment, we can also observe the same asymmetric line shape in the transmission spectrum of the PhC slab except for a slight redshift due to the fabrication imperfection. In addition, as shown in Fig. 3b, the Fano resonance is highly tunable by changing the parameters of the PhC (e.g. Λ and r).

2. Device fabrication

The device was fabricated on a commercially available suspended silicon nitride (SiN) membrane (thickness h=100 nm). The photonic crystal was patterned by the E-beam lithography (EBL) and followed by the reactive-ion etching (RIE) with the CHF_3/O_2 chemistry until the SiN membrane was totally etched through. Finally the CVD-grown single crystal MoS_2 flakes were transferred onto the suspended SiN photonic crystal membrane.

3. Device Characterization

To measure the transmission spectra of the devices, a broad band white light source was illuminated on the sample in the normal direction (z axis), and the transmitted light was collected by a 40X (NA=0.6) objective and measured by a spectrometer with a cooled charge-coupled device (CCD) camera. For the PL intensity measurement, the MoS_2 samples were optically pumped by the continuous wave (CW) 532 nm or 633 nm lasers. Two objectives were respectively used to focus the laser beam as a comparison: 10X (NA=0.3) and 40X (NA=0.6) objectives. The PL emission were measured by the spectrometer with a CCD camera. To measure the PL far field pattern, the rear focal plane of the objective (100X, NA=0.9) was projected onto the cooled CCD by a Fourier lens. To measure the angular dispersion of the Fano resonant PhC slab, the far field emission was dispersed by the spectrometer and imaged on the CCD camera. The horizontal axis displays the emission wavelength and the vertical axis corresponds to the emission angle[2].

4. The PL spectra of the SiN substrate and the MoS_2 monolayer on the SiN substrate

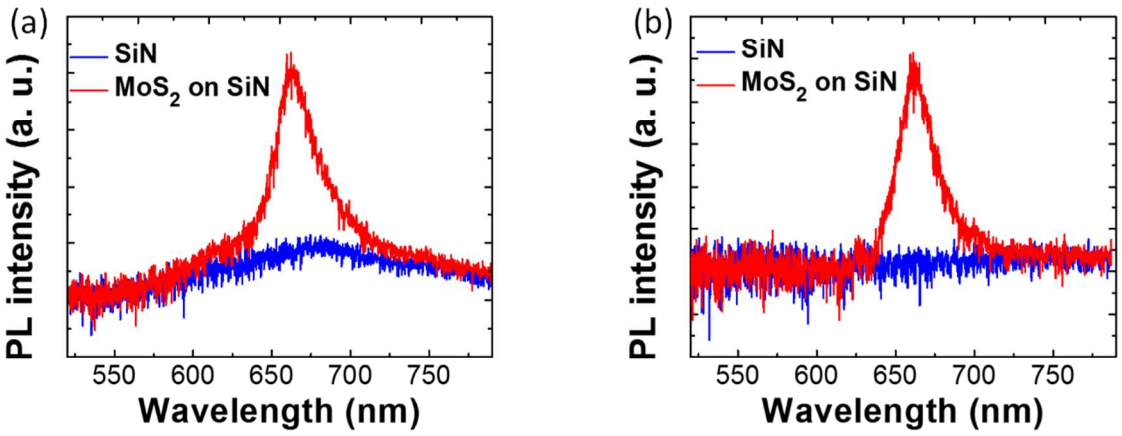

Figure S4. The PL spectra of the SiN substrate and the MoS_2 monolayer on the SiN substrate: (a) the samples were pumped by a 532 nm CW laser, and the PL from SiN can be observed (blue curve). To obtain the PL of the MoS_2 monolayer, the SiN PL background was removed from the PL of the MoS_2 monolayer on SiN substrate (red curve); (b) the samples were pumped by a 633 nm CW laser, and no PL of the SiN was observed.

5. The photoluminescence enhancement analysis

There are five factors related to photoluminescence (PL) enhancement of the MoS_2 monolayer: (i) the pump light absorbance enhancement: η_a; (ii) the intrinsic PL efficiency enhancement: η_i; (iii) the Purcell effect related spontaneous emission rate enhancement: η_s; (iv) the upward light extraction efficiency enhancement: η_e; (v) the angular collection efficiency enhancement: η_c. The total PL enhancement is determined by their product $\eta_t=\eta_a\times\eta_i\times\eta_s\times\eta_e\times\eta_c$. In this work, the MoS_2

monolayer on the substrate (the unpatterned SiN slab: n=2.17, thickness h=100 nm) was used as the reference. All five enhancement factors were investigated through the 3D FDTD simulations with a commercial FDTD software (Lumerical FDTD Solutions).

a. **The pump light absorbance enhancement (η_a).** A broad band plane wave was launched onto the PhC slab integrated with MoS_2 monolayer, and the electric field distribution was calculated by the 3D FDTD simulation in a unit cell with the periodic boundary conditions. Then the pump light absorbance in the monolayer is calculated $A_{PhC} = \frac{1}{2}\iiint |E|^2 \, Im(\varepsilon) \, dV$, where E is the electric field intensity at a given position and ε is the permittivity at that point. The same calculation was also performed for the reference sample (A_{ref}), and the ratio ($\eta_a = A_{PhC}/A_{ref}$) yields a pump light absorbance enhancement of η_a=6 at λ=532 nm and η_a=13 at λ=633 nm.

b. **The Purcell effect enhancement of the spontaneous emission (η_s).** It is noted that the spontaneous emission rate of a fluorophor can be modified by its environment via the Purcell effect. To investigate the spontaneous emission rate modified by the Purcell effect, a dipole was placed on a PhC slab and an unpatterned SiN slab, respectively. Considering the calculation accuracy, a large simulation volume of 16×16×2 μm^3 (i.e. 31×31 unit cells) was used. Due to the memory and computational time limitations of our workstation, the atomically thin MoS_2 monolayer, was not included in this simulation. In our case, this simplification is reasonable because the only effect of the MoS_2 monolayer on the PhC slab is a small red shift of the Fano resonance (Fig. 1b). The total output power (P_{out}) normalized to the power emitted by the dipole in free space (P_0) is the spontaneous emission rate related to the Purcell effect ($S = P_{out}/P_0$). For the calculation of the PhC slab, the same calculation was

performed by placing the dipole at different positions and the resulting spontaneous emission rates were averaged. Finally, the ratio $\eta_s = S_{PhC}/S_{ref}$ yields the Purcell factor and the spontaneous emission rate enhancement $\eta_s=3$ at $\lambda=650$ nm.

c. **The upward light extraction efficiency enhancement (η_e).** Due to the symmetry of the PhC, not all the power output by the dipole can be emitted upwards. Following the calculation in b, the upwards emitted power (P_{up}) normalized to the total output power (P_{out}) in all directions represents the extraction efficiency (P_{up}/P_{out}). The same calculation was performed for both the PhC (E_{PhC}) and unpatterned SiN slab (E_{ref}), and the ratio $\eta_e = E_{PhC}/E_{ref}$ is the upward light extraction efficiency enhancement ($\eta_e=8$ at $\lambda=650$ nm).

d. **The angular collection efficiency enhancement (η_c).** It is noted that the numerical aperture (NA) of the detection system is normally less than 1 in air. Therefore, considering the angular emission of the sample, not all MoS_2 monolayer PL photons can be collected due to the mismatch between the NA and the radiation pattern of the monolayer. To calculate the angular collection efficiency within a particular solid angle, the far field emission pattern for the sample was calculated by following the calculation in b. The angular collection efficiency is calculated by normalizing the emitted power within a certain solid angle (corresponding to the NA) to the entire upward emitted power (P_{angle}/P_{up}). The same calculation was performed for both the PhC (C_{PhC}) and the unpatterned SiN slab (C_{ref}), and the ratio $\eta_c = C_{PhC}/C_{ref}$ is the angular collection efficiency enhancement ($\eta_c=1.1$ for NA=0.6, and $\eta_c=1.8$ for NA=0.3). We note that the enhancement here is larger for the lower NA case. This is due to the fact that the emission from the dipole on the PhC is highly directional, while it is highly isotropic on the unpatterned substrate. This result indicates that the power collected from the unpatterned sample increases significantly with increasing NA as this offers a better overlap with the

large emission solid angle. On the contrary, the emission from the PhC can be highly directional and is not as sensitive to the collection NA. In summary, this supports that for the case of the monolayer on the PhC even a low NA collection optics can offer significant efficiency.

e. **The intrinsic PL efficiency enhancement (η_i).** Due to the n-doping and the defect-assisted non-radiative exciton recombination from the substrate, the intrinsic quantum yield of the MoS_2 monolayer on the substrate is up to 2 orders of magnitude smaller than that of the suspended MoS_2 monolayer[3, 4]. To obtain this intrinsic chemical PL efficiency enhancement of the suspended MoS_2 monolayer against the MoS_2 monolayer on the unpatterned SiN substrate, the geometry dependent electromagnetic enhancement factors (i.e. η_a, η_s, η_e, and η_c) have to be taken into account for the suspended structure and the substrate. For this purpose, we first measured the PL spectra of both the MoS_2 monolayer suspended in the air and on the substrate with the same pump intensity (Fig. 2b). Then we divided the PL spectra of the MoS_2 monolayer suspended in the air by that of the MoS_2 monolayer on the substrate and obtained the total PL enhancement with a peak enhancement of η_t=45 at λ=650 nm (Fig.S5a). However, this number already includes the different laser absorbance on the substrate, etc. Therefore one needs to consider the electromagnetic effects due to the substrate in order to determine the true intrinsic quantum yield enhancement (i.e. chemical) for the suspended monolayer. The enhancement factors for the suspended MoS_2 monolayer η_a, η_s, η_e, and η_c were calculated by following the calculation procedures used for a-d above (Fig. S5b). Finally, the intrinsic PL efficiency enhancement (η_i) was obtained after correcting for η_a, η_s, η_e, and η_c (Fig. 2c). The peak intrinsic chemical PL efficiency enhancement (η_i) is 9 at λ=650 nm. When integrated with the PhC slab, the MoS_2 monolayer is only partially

suspended. For the PhC slab used in the experiment (Λ=470 nm, r=160 nm), the filling fraction (FF=$\pi r^2/\Lambda^2$) is 36%, which means only 36% of the MoS_2 monolayer is suspended in the air. Therefore, the spatially averaged peak intrinsic PL efficiency enhancement of the MoS_2 monolayer integrated with the PhC slab is 0.36×9+0.64×1=3.9 (λ=650 nm).

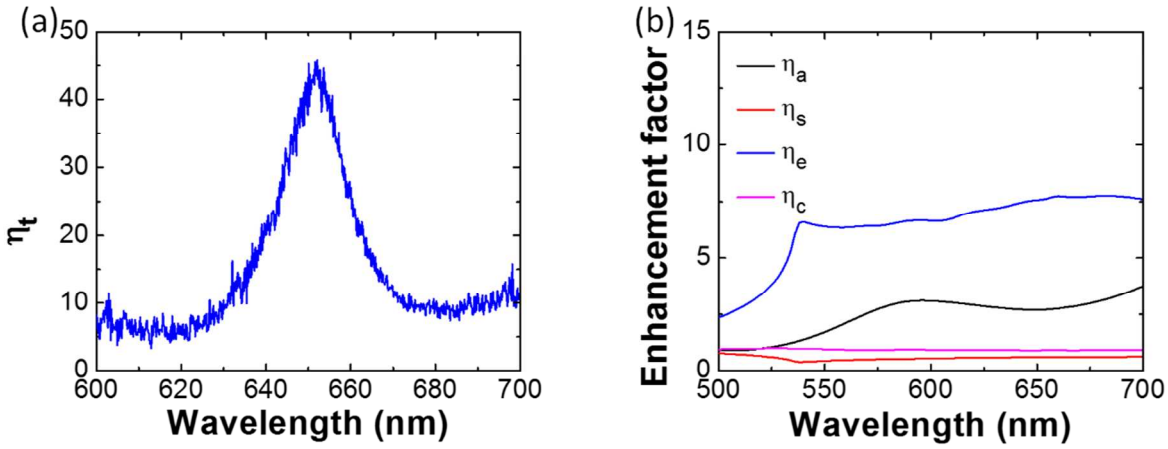

Figure S5. (a) The total PL enhancement of the suspended MoS_2 monolayer (η_t) obtained by dividing the PL spectra of the MoS_2 monolayer suspended in the air by that of the MoS_2 monolayer on the substrate. (b) The FDTD calculated electromagnetic PL enhancement factors for the MoS_2 monolayer suspended in the air: the pump laser absorption enhancement (η_a), the Purcell effect enhancement of spontaneous emission rate (η_s), the upward light extraction efficiency enhancement (η_e), and angular collection efficiency enhancement (η_c).

In summary, all of these enhancement factors η_a, η_s, η_e, η_c, and η_i for the MoS_2 monolayer integrated with the PhC slab were calculated by following the calculation procedure above yielding a total PL enhancement $\eta_t=\eta_a\times\eta_i\times\eta_s\times\eta_e\times\eta_c$ (Table S1 and Fig. S6).

Table S1. The summary of calculated values for the Fano resonant PL enhancement factors

η_a	η_i	η_s	η_e	η_c	η_t
6 (532 nm excitation) 13 (633 nm excitation)	3.9*	3*	8*	1.8* (NA=0.3) 1.1* (NA=0.6)	617* (532 nm excitation, NA=0.6) 1338* (633 nm excitation, NA=0.6) 2190* (633 nm excitation, NA=0.3)

*These are the enhancement factors at λ=650 nm.

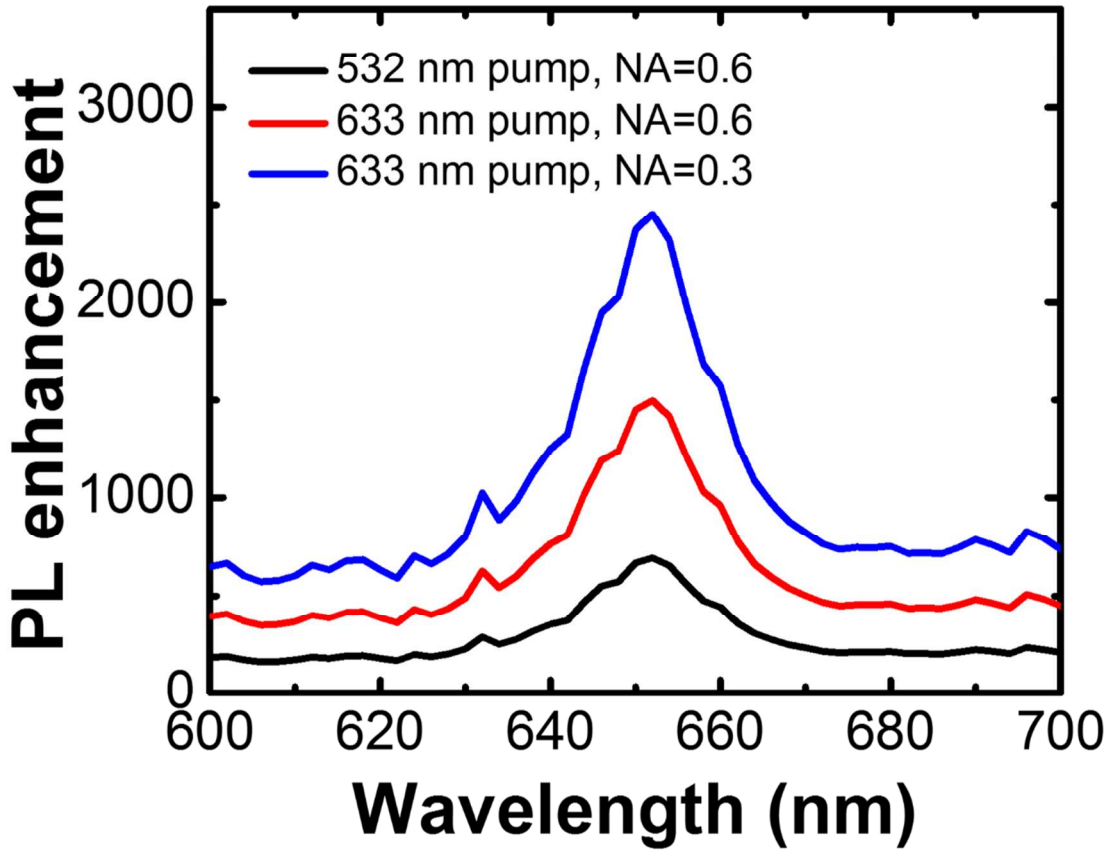

Figure S6. The theoretically predicted wavelength dependent MoS_2 PL enhancement via the photonic Fano resonances.

6. The angular emission properties of the MoS_2 monolayer on the substrate

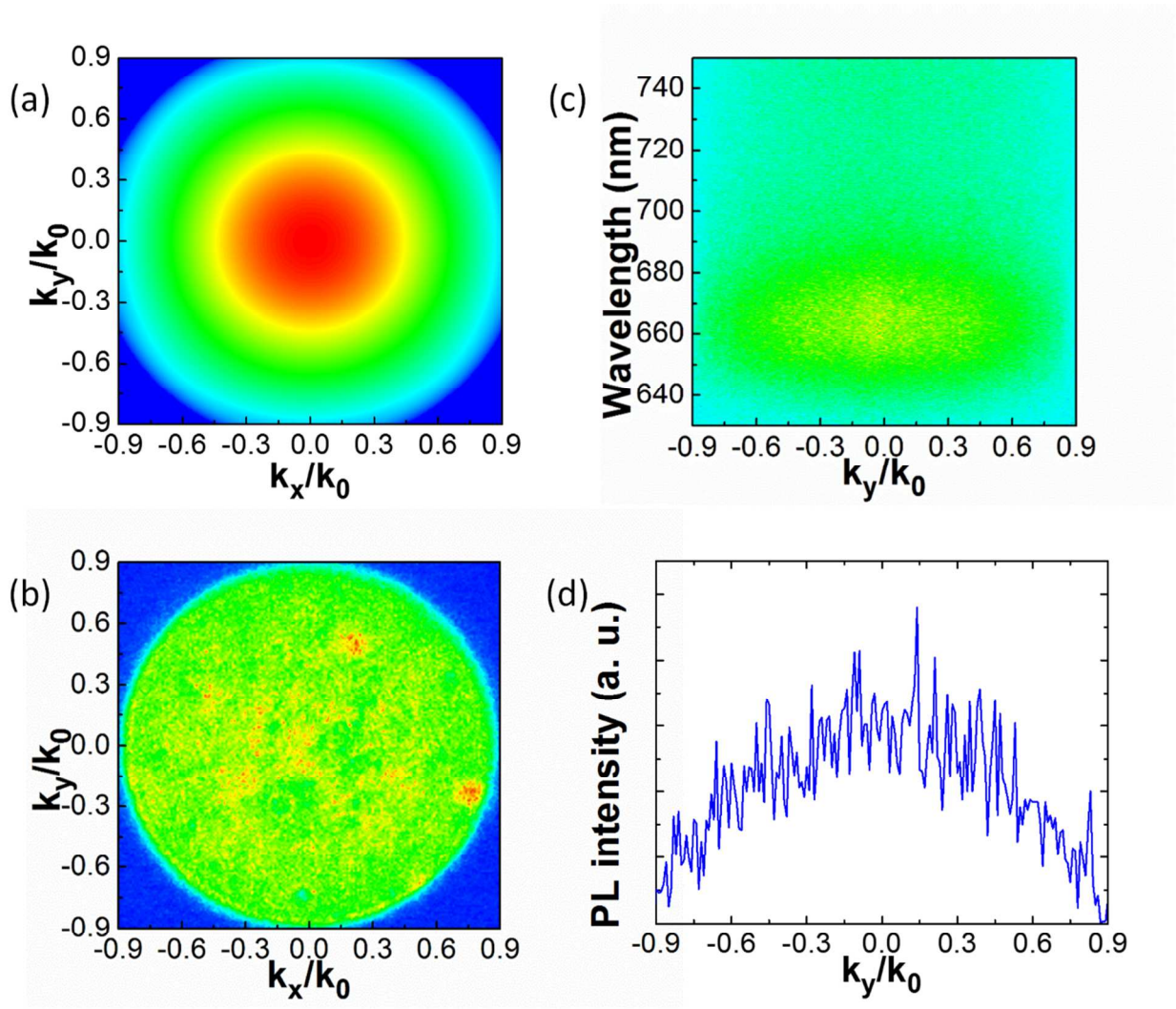

Figure S7. The angular emission properties of the MoS_2 monolayer on the substrate (i.e. unpatternded SiN slab): the calculated (a) and measured (b) far field distributions of the MoS_2 monolayer on the substrate; the measured (c) angular photoluminescence emission spectra exhibits no angular dispersive behavior; (d) the measured angular PL emission at A exciton peak (λ=650 nm).

7. The MoS_2 PL spectra at different emission angles

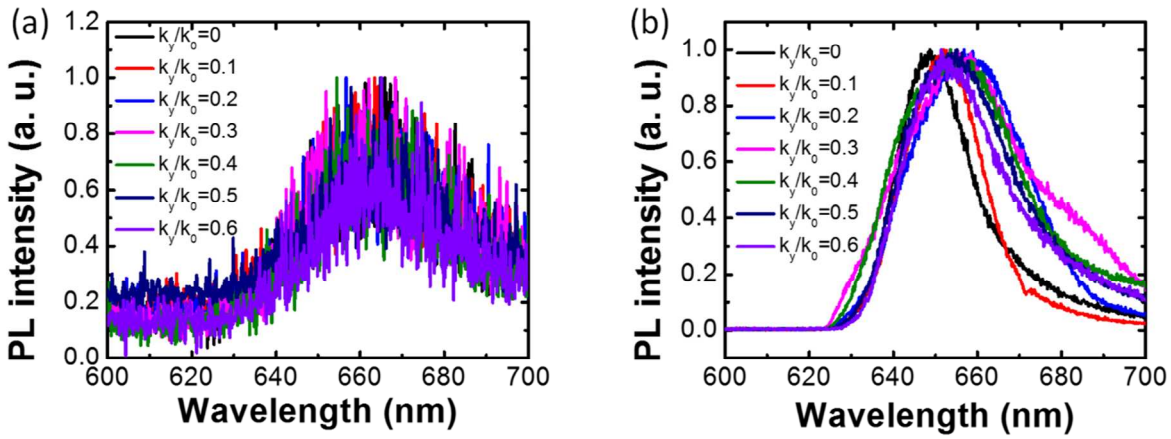

Figure S8. The MoS_2 PL spectra at different emission angles: (a) MoS_2 on the substrate (unpatterned SiN, thickness=100 nm). The spectra are extracted from Fig. S7c; (b) MoS_2 on the PhC slab. The spectra are extracted from Fig. 4b.

As can be seen in the Fig. S8, larger PL emission above λ=670 nm can be observed at larger emission angles (i.e. k_y/k_0=0.3, 0.4, 0.5, 0.6) for the MoS_2 on the PhC slab. In contrast, no angular dependent emission can be found for the MoS_2 on the substrate. Therefore, when an objective with NA=0.6 is used, in addition to the PL enhancement peak at λ=650 nm, there is a bump in the PL enhancement spectrum between λ=670 nm and λ=700 nm, because the enhanced PL emission with larger emission angles (i.e. k_y/k_0=0.3, 0.4, 0.5, 0.6) can be collected by the objective with NA=0.6. However, when an objective with NA=0.3 is used, the bump in the PL enhancement spectrum between λ=670 nm and λ=700 nm will be weakened because the enhanced PL emission with larger emission angles can not be collected.

8. The demonstration of the PL enhancement for the device used in Fig. 5

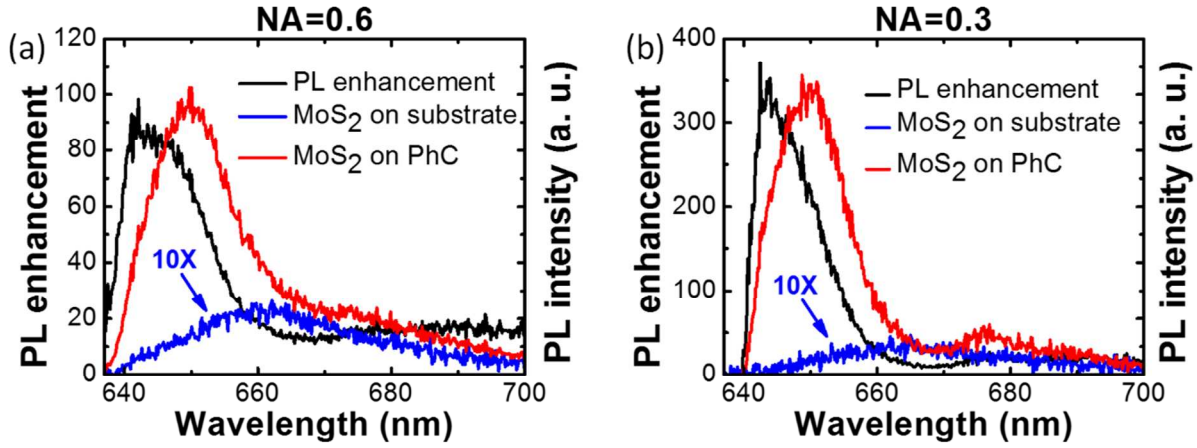

Figure S9. The experimental demonstration of the Fano resonance enhanced photoluminescence of the device used in Fig. 5: objectives with NA=0.6 (a) and NA=0.3 (b) were used in the experiment. The excitation laser wavelength was 532 nm. The PL spectrum of the MoS_2 on the substrate is scaled by a factor of 10 for the visual convenience.

Table S2. The PL enhancement comparison of two devices used in this work*

Device	η_a	η_i	η_s	η_e	η_c	η_t(theoretical)	η_t(experimental)
Λ=470nm; r=160nm	6	3.9*	3*	8*	1.1*	617*	300*
Λ=450nm; r=120nm	3.7	2.8*	2*	5*	1.1*	114*	70*

*pump laser: 532 nm CW laser; Objective: NA=0.6

**These are the enhancement factors at λ=650 nm.

9. The analysis of forward/backward MoS_2 emission

For both cases with MoS_2 on an unpatterned and a patterned SiN slab, there is emission in both forward and backward directions (Fig. S10a). However, the emission is asymmetric, since the MoS_2 monolayer is on the top side of the SiN slab. For both the PhC slab and the unpatterned SiN slab, the forward light extraction efficiencies are larger than those in the backwards direction. Compared to the unpatterned SiN slab, both forward and backward extraction efficiencies are enhanced for the PhC case as illustrated in Fig. S10b. We note for the PhC case there is more light emitted in the forward than the backward direction, which is the opposite of the bare slab case. This further emphasizes the advantage of the PhC Fano resonance for directional emission.

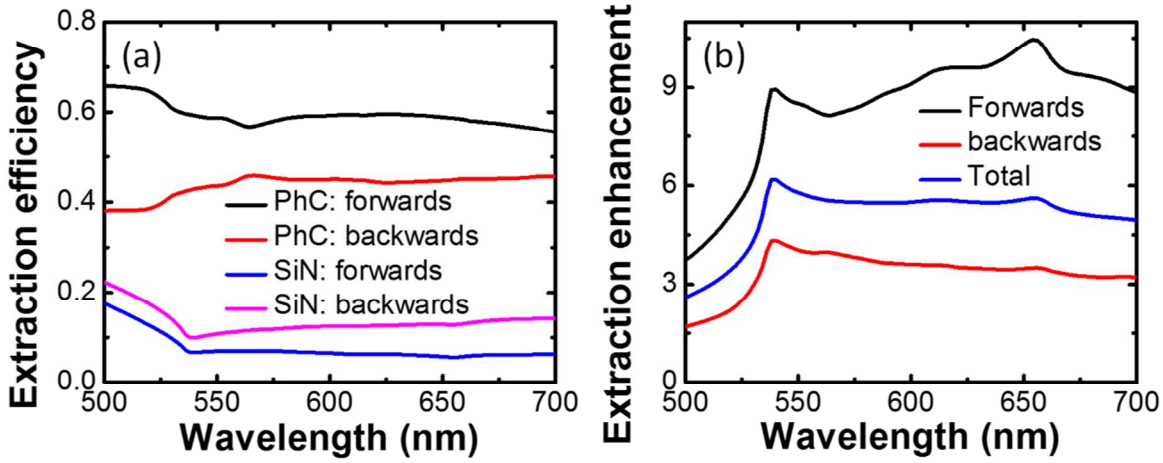

Figure S10. (a) The calculated forward and backward light extraction efficiencies for both the PhC slab and the unpatterned SiN slab. (b) The light extraction enhancement for the PhC slab. The unpatterned SiN slab is used as the reference. For these calculation, a single dipole is placed in the center of the hole, which is a simplification of the calculation used in Section 5.

To further enhance the MoS_2 emission, the PhC slab can be coated with a 100 nm thick Ag layer on the backside. The Ag layer can significantly alter the PhC Fano resonance, therefore we tune the PhC period to make sure the PhC Fano resonance matches the pump laser wavelength. As shown in Fig. S11, for the PhC slab with Ag coating, the Fano resonance mode around 532 nm disappears. However, due to the back reflection of the pump laser from the Ag coating, the absorption enhancement (η_a) at 633 nm becomes 27 times, which is ~2x that of the PhC slab without Ag coating (Table S3). On the other hand, due to the larger hole period, the hole filling fraction for the PhC slab with Ag coating is smaller ($FF=\pi r^2/\Lambda^2=0.26$), so that the intrinsic chemical enhancement (η_i) from the suspended MoS_2 monolayer is expected to decrease (Table S3). We also calculate the Purcell effect enhancement of the spontaneous emission (η_s), the out-of-plane light extraction enhancement (η_e) and the angular collection efficiency enhancement (η_c). For these calculations, we place a single dipole in the center of the hole which is a simplification for the calculation in Section 5. This is a valid simplification since our primary interest is the PL enhancement ratio for the PhC slab with and without the Ag coating. As can be seen in Fig. S11b, the Purcell effect enhancement (η_s) for the PhC slab with Ag coating is slightly smaller than that of the PhC slab without Ag coating in the PL spectral range (~650 nm). Besides, the PhC slab with Ag coating has a much larger out-of-plane light extraction enhancement (η_e), which is also attributed to the back reflection of the pump laser from the Ag coating. However, the PhC slab with Ag coating has a smaller angular collection efficiency (Table S3). Considering all of the above PL enhancement mechanisms, the total PL enhancement for the PhC slab with Ag coating is 1.5 times larger than the one without Ag coating, although with a different set of optimized geometric parameters.

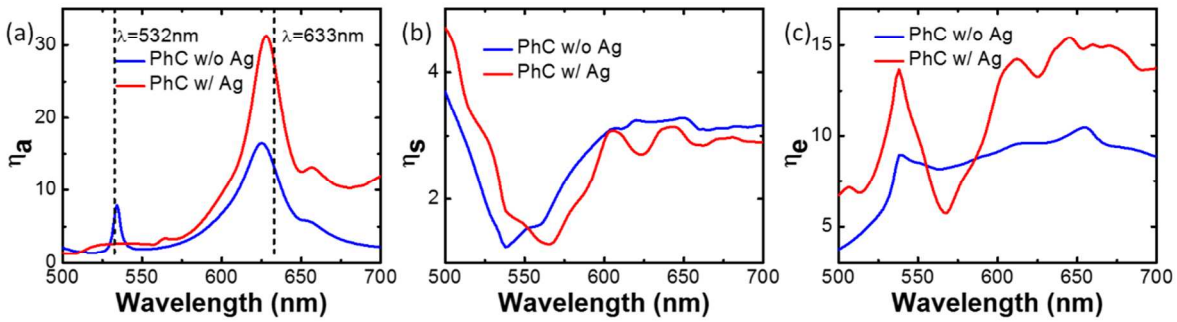

Figure S11. (a) The calculated absorption enhancement (η_a), (b) the Purcell effect enhancement (η_s), and (c) out-of-plane light extraction enhancement (η_e) for a monolayer on a PhC slab without and with the 100 nm thick Ag back reflector. For the calculation in (b) and (c), a single dipole is placed in the center of the hole, which is a simplification for the calculation used in Section 5.

Table S3. The PL enhancement comparison of PhC w/o and w/ Ag coating*

Device	Parameters	η_a#	η_i‡	η_s†,‡	η_e†,‡	η_c†,||,‡	η_t‡
PhC slab w/o Ag coating	Λ=470nm; r=160nm	13	3.9	3.3	10	1.8	3012*
PhC slab w/ Ag coating	Λ=560nm; r=160nm	27	3.1	3.0	15	1.2	4520*

*Ag thicknes is 100 nm

#Calculated at 633 nm

†A dipole is placed in the center of the hole

|| Objective (NA=0.3) is used

‡These are the enhancement factors at λ=650 nm.

10. The deconvolution of MoS_2 photoluminescence spectrum

The MoS_2 PL spectrum between 620 nm and 700 nm can be fitted by two Lorentz functions. As shown in Fig. S12, the sum of the two fitting curves matches the experimental results very well. In this way, the MoS_2 PL spectrum is decovoluted into A exciton emission and A^- trion emission with peak positions of 650 nm and 670 nm, respectively.

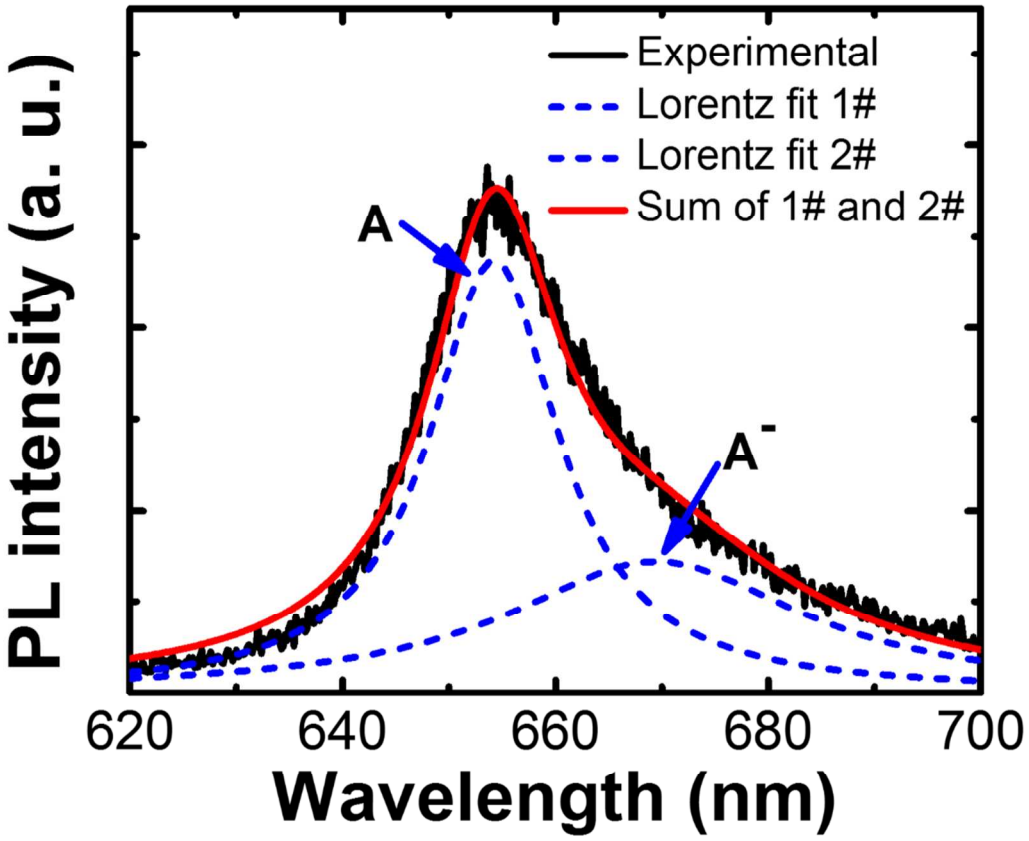

Figure S12. The photoluminescence of suspended MoS_2 monolayer (black line). Blue dotted lines show the Lorentz functions of A exciton and A^- trion. Red line is the sum of the blue dotted lines.

11. The Gaussian beam propagation

We simulate the focused laser beam (λ=532nm) for the 0.6 NA objective. Due to the high degree of spatial coherence of the laser, a Gaussian beam, an approximation to the Airy beam, is formed at the focal plane (y=0). The laser beam will diverge when the sample is far from the focal plane. But when the sample is near to the focal plane, the divergence angle is very small.

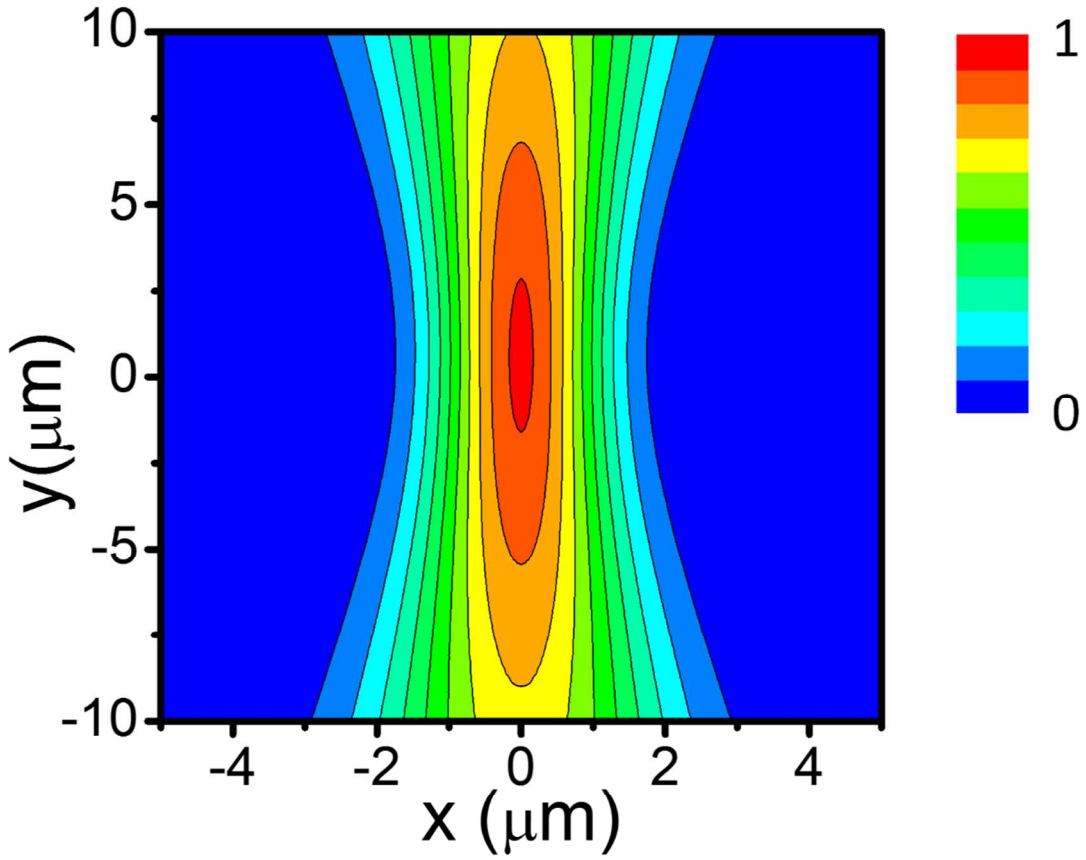

Figure S13. The contour plot of the Gaussian beam propagation (NA=0.6). The polarization of electric field is along the x axis. The Gaussian beam (λ=532 nm) propagates along the y axis and focus at y=0 plane.

12. Band structure of the photonic crystal slab

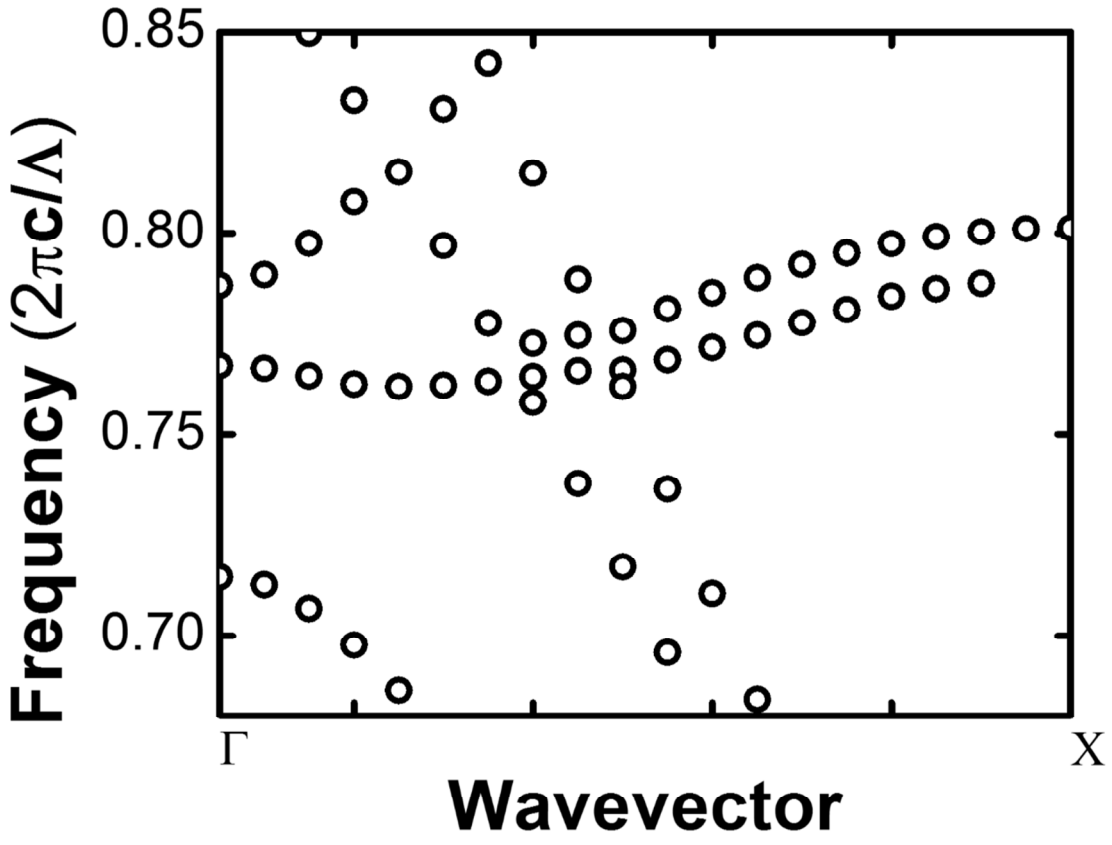

Figure S14. Partial band structure of the SiN PhC slab (thickness h=100nm, hole period Λ=470nm, hole radius r=160nm).

References

1. Fan, S.; Suh, W.; Joannopoulos, J. D. *J. Opt. Soc. Am. A* **2003,** 20, (3), 569-72.
2. Liu, W.; Lee, B.; Naylor, C. H.; Ee, H. S.; Park, J.; Johnson, A. T.; Agarwal, R. *Nano Lett.* **2016,** 16, (2), 1262-9.

3. Yu, Y.; Yu, Y.; Xu, C.; Cai, Y.-Q.; Su, L.; Zhang, Y.; Zhang, Y.-W.; Gundogdu, K.; Cao, L. *Adv. Funct. Mater.* **2016,** 26, (26), 4733-4739.
4. Scheuschner, N.; Ochedowski, O.; Kaulitz, A.-M.; Gillen, R.; Schleberger, M.; Maultzsch, J. *Phys. Rev. B* **2014,** 89, (12), 125406.